



**HAL**  
open science

## Impact of transient groundwater storage on the discharge of Himalayan rivers

Christoff Andermann, Laurent Longuevergne, Stéphane Bonnet, Alain Crave, Philippe Davy, Richard Gloaguen

### ► To cite this version:

Christoff Andermann, Laurent Longuevergne, Stéphane Bonnet, Alain Crave, Philippe Davy, et al.. Impact of transient groundwater storage on the discharge of Himalayan rivers. *Nature Geoscience*, 2012, 5, pp.127-132. 10.1038/NGEO1356 . hal-00710433

**HAL Id: hal-00710433**

**<https://hal.science/hal-00710433>**

Submitted on 21 Jun 2012

**HAL** is a multi-disciplinary open access archive for the deposit and dissemination of scientific research documents, whether they are published or not. The documents may come from teaching and research institutions in France or abroad, or from public or private research centers.

L'archive ouverte pluridisciplinaire **HAL**, est destinée au dépôt et à la diffusion de documents scientifiques de niveau recherche, publiés ou non, émanant des établissements d'enseignement et de recherche français ou étrangers, des laboratoires publics ou privés.

# 1 **Impact of transient groundwater storage on the discharge of** 2 **Himalayan rivers**

3

4 Christoff Andermann<sup>1,2</sup>, Laurent Longuevergne<sup>1</sup>, Stéphane Bonnet<sup>3</sup>, Alain Crave<sup>1</sup>, Philippe Davy<sup>1</sup> and  
5 Richard Gloaguen<sup>2</sup>

6

7 <sup>1</sup> Géosciences Rennes, Université de Rennes 1, CNRS, Campus de Beaulieu, 35042 Rennes, France

8 <sup>2</sup> Remote Sensing Group, Geology Institute, TU Bergakademie Freiberg, B.-von-Cotta-Str. 2, 09599  
9 Freiberg, Germany

10 <sup>3</sup> Géosciences Environnement Toulouse, Université de Toulouse, CNRS-UPS-IRD, Observatoire Midi-  
11 Pyrénées, 14 Av. Edouard Belin, 31400 Toulouse, France

12

13 Corresponding author:

14 Christoff Andermann,

15 Tel (+33) 2 23 23 66 24

16 christoff.andermann@univ-rennes1.fr

17

18 **The transfer of precipitation into rivers involves temporary water storage in reservoirs<sup>1,2</sup> such as**  
19 **soils, groundwater, snow and glaciers, where different residence times influence the hydrological**  
20 **cycle. In the central Himalayas, the water budget is considered to be primarily controlled by**  
21 **monsoon rainfall, snow and glacier melt<sup>3,4</sup>, and secondarily by evapotranspiration<sup>3</sup>. The**  
22 **existence of a deep groundwater contribution<sup>5-7</sup> is deduced from the chemistry of Himalayan**  
23 **rivers<sup>6</sup>. However, its importance in the annual water budget remains to be evaluated. Here, we**  
24 **analyze ~30 years of daily precipitation and discharge within major catchments in Nepal. We**  
25 **observe annual precipitation-discharge hysteresis loops, in both glaciated and unglaciated**  
26 **catchments, independently of the geological setting. This implies the temporal storage of water in**

27 a reservoir whose characteristic response time ( $\sim 45$  days) represents a typical diffusivity ( $\sim 1 \text{ m}^2 \text{ s}^{-1}$ ) of fractured basement aquifers<sup>8</sup>. This transient storage capacity is of  $\sim 28 \text{ km}^3$  for the three  
28 main catchments of Nepal, whereas we estimate snow and glacier melt contribution to be  $\sim 14$   
29  $\text{km}^3 \text{ yr}^{-1}$  ( $\sim 10\%$  of the annual river discharge). We conclude that groundwater storage in  
30 fractured basement constitutes an important compartment of the Himalayan river discharge  
31 cycle, that can be quantified through the study of precipitation and discharge throughout the  
32 year.  
33

34

35 The discharge of the central Himalayan rivers is governed by a strong precipitation seasonality  
36 <sup>3,6,9,10</sup> (Fig. 1) with up to 80% of the annual rainfall occurring during the Indian Summer Monsoon  
37 (ISM) season<sup>3</sup>. The ISM precipitation is the main source for glacier mass accumulation<sup>9</sup> and its spatial  
38 distribution is strongly influenced by orographic effects<sup>3</sup>. Variations in intensity and duration of the  
39 ISM, linked to El Nino/Southern Oscillation (ENSO)<sup>11</sup>, enhance the annual amount of precipitation by  
40  $\sim 25$  to 50% with respect to the annual mean at low to moderate elevation ( $>3 \text{ km}$ ), and up to 200% at  
41 high elevation<sup>12</sup>. Snowmelt contributes to a significant fraction of river discharge in the western and  
42 eastern Himalayas and on the Tibetan plateau<sup>3,13</sup>, but only to a minor fraction ( $\sim 10\%$ ) in the central  
43 Himalayas, mainly in the early ISM (May to July)<sup>3</sup>. It has been suggested that rainfall-derived  
44 discharge, ice and snowmelt are the primary factors controlling Himalayan river discharge, with  
45 evapotranspiration forming a secondary minor component<sup>3</sup>. Notwithstanding, this hydrological budget  
46 model neglects transient water storage in soils, floodplains and groundwater. However, geochemical  
47 data indicate that a non-negligible part of surface runoff originates from deep groundwater reservoirs<sup>6</sup>.

48

49 We investigate the transfer of water within the main catchments of the Nepal Himalayas (Fig.  
50 1a) using a daily meteorological and hydrological dataset spanning  $\sim 30$  years (Table 1). We consider  
51 the three main catchments of Nepal (Sapta Koshi, Narayani and Karnali basins), some of their  
52 tributaries, and three unglaciated small catchments at the front of the Himalayan range (Fig. 1a and  
53 Table 1). The main catchments drain the entire Himalayan range of Nepal, from the Tibetan Plateau to  
54 the Lesser Himalayas. Most of their headwaters are located on the arid Plateau (Fig. 1a), characterized

55 by a weaker influence of the ISM. The rivers incise bedrock comprising, from north to south, the low-  
56 grade Paleozoic-Mesozoic Tethyan Sediment Series, high-grade metamorphic gneisses and migmatites  
57 of the High Himalayan Crystalline Series and low-grade Proterozoic sediments of the Lesser  
58 Himalayas (Fig. 1c). Most of the data considered here come from outlet stations located to the north of  
59 the Siwalik foreland. The annual specific discharge of the studied basins is typically on the order of  
60  $\sim 10^3$  mm yr<sup>-1</sup> (Table 1) and their annual hydrograph clearly shows the seasonal impact of the ISM on  
61 river discharge, generally peaking in July/August<sup>3,14</sup> (Fig. 1b). Mean annual basin precipitation is 920,  
62 1396 and 920 mm yr<sup>-1</sup> in the Sapta Koshi, Narayani and Karnali catchments, respectively. However,  
63 precipitation is spatially heterogeneous (Fig. 1a) and is strongly controlled by orography, reaching a  
64 maximum between elevations of 2 to 3 km<sup>15,16</sup>. The upper parts of the catchments are glaciated (Fig.  
65 1a), covering between 4 and 15 % of the catchment area (Table 1).

66

67 We calculated mean basin-wide daily precipitation rate and use daily discharge measurements  
68 to compute specific water discharge for all the studied drainage basins (see Methods). Plots of daily  
69 precipitation vs. specific discharge highlight a considerable scatter within the  $\sim 30$  year dataset (Fig.  
70 2a). However, the chronology of the data exhibits a well-defined annual cycle, showing an increase of  
71 discharge with increasing precipitation during pre-ISM (March-May) to ISM (June-September) and a  
72 decrease during post-ISM (October-November). The systematic higher discharge for a given  
73 precipitation rate during post-ISM compared with pre-ISM is striking. The data consequently shows an  
74 annual anticlockwise hysteresis loop (Fig. 2a). A 30-day moving average highlights the temporal  
75 consistency of the loop from year to year (Fig. 2a, inset). Data scattering results from inter-annual  
76 variability, particularly during post-ISM, as illustrated by comparing the data during a strong or a weak  
77 ISM year (see Supplementary Fig. S1). The annual anticlockwise hysteresis loop is observed in all  
78 studied basins (Fig. 2b), regardless of the geological units, the presence of glaciers or snow cover  
79 (Tab. 1).

80

81 Anticlockwise hysteresis loops imply that precipitation is temporarily stored within the  
82 catchments and not transferred directly to the river during pre-ISM and ISM seasons, whereas the

83 storage compartment is drained during post-ISM. Glaciers can be directly ruled out as the main  
84 contributor to the observed hysteresis effect because the release of water by glacier or snow melt  
85 occurs principally during pre-ISM to ISM season<sup>3,13</sup> (Fig. 3b and S2), which is not consistent with the  
86 anticlockwise nature of the hysteresis. Moreover, hysteresis effects are observed in both glaciated and  
87 unglaciated catchments (Fig. 2b). As the potential evapotranspiration in the Himalayas reaches a  
88 maximum during pre-ISM, in April-May<sup>17</sup> (Fig. 1b), this could qualitatively explain the anticlockwise  
89 hysteresis loop. However, it is estimated to account for less than 10% of the overall hydrological  
90 budget<sup>3</sup>, so this effect plays likely a minor role, mainly because the magnitude of evapotranspiration  
91 rapidly decreases with elevation<sup>17</sup>. Consequently, the main mechanism explaining the hysteresis effect  
92 is likely a transient storage of water in a groundwater unit during the rising ISM and its post-ISM  
93 release.

94

95 To precise the role of groundwater storage on the Himalayan hydrological cycle, we solved the  
96 water balance at catchment scale in order to discriminate time response distribution in discharge data  
97 and relate it to storage compartments via hydrological modeling. We used a modified version of the  
98 conceptual hydrological model GR2M (see Methods), which addresses several physical processes in a  
99 simplified, but proven robust, way in a wide range of climatological settings<sup>18</sup>. Because the observed  
100 hysteresis effect is a seasonal process, daily modeling of hydrological processes is not the pertinent  
101 scale for our purpose (see ref. 19). The large diversity of involved processes, within a wide range of  
102 environmental settings, limits the reliability of short-term modeling so we modeled the data at a  
103 monthly rather than at a daily scale. Note, that we nevertheless tested daily scale modeling (see  
104 Methods and Supplementary Table S1). Modeled daily results are generally similar to monthly ones  
105 (Table 1), but the efficiency is however less well described (Table 1 and Supplementary Table S1). The  
106 model simulates the catchment response to rainfall in terms of river discharge and incorporates three  
107 components (see supplementary figure S3): 1) a snow module based on the HBV approach<sup>20</sup> (see  
108 Methods), 2) a fast rain-to-discharge flow related to quick runoff processes, and 3) a slow flow  
109 component representing groundwater contribution. This third reservoir retards the rain-discharge  
110 response and yields baseflow during dry periods. It is characterized by a response time  $t_c$ , defined as

111 the time for a hydrological system to reach equilibrium after the hydraulic head has changed<sup>1</sup>. The  
112 model is forced by precipitation, temperature and potential evapotranspiration (see Methods). We  
113 calibrated on the logarithm of all the observed daily water discharge to account for the large range of  
114 discharges, *i. e.* to apply identical weights to both high and low water stages, and under the constraint  
115 that total observed and modeled discharge volumes are identical. The modeling is robust in most  
116 catchments: hysteresis loops are confidently reproduced for all catchments (e. g. Supplementary Fig.  
117 S4) with Nash-Sutcliffe coefficients of 0.89, 0.91 and 0.92 for Sapta Koshi, Narayani and Karnali  
118 basins, respectively (Table 1). The modeling implies a significant storage of water within the slow  
119 flow reservoir, with calculated  $t_c$  longer than one month (Table 1). Modeled data are in agreement with  
120  $t_c$  values derived directly from the fit of baseflow recession curves<sup>21</sup> (see Methods and Table 1). This  
121 delay between precipitation and discharge yields baseflow during dry periods and is responsible for  
122 the existence of the hysteresis loops. Shorter  $t_c$ , associated with a low storage capacity (e.g. 10 days  
123 equivalent to 20 times smaller storage capacity), do not allow to reproduce the observed hysteresis  
124 loops analytically (see Methods and Supplementary Fig. S5c).

125

126 The nature of the groundwater system controlling the hysteresis effect is provided by its  
127 response time  $t_c$ . For groundwater systems,  $t_c$  is inversely proportional to the hydraulic diffusivity  $D$   
128 (transmissivity divided by storage coefficient) and is proportional to the square of the characteristic  
129 aquifer scale  $L_c$ :  $t_c \sim L_c^2 * D^{-1}$  <sup>ref 1</sup>.  $L_c$  is the characteristic distance between the aquifer and streams, which  
130 is approximately the hillslope length if aquifers are spread homogeneously over the drainage basin.  
131 Considering  $L_c$  in the range 0.5–5 km and  $t_c$ , of ~45 days, equivalent diffusivity values are about ~1 m<sup>2</sup>  
132 s<sup>-1</sup>, a typical value of aquifers in fractured rocks<sup>8</sup> (0.01 to 10 m<sup>2</sup> s<sup>-1</sup>). Recession curve exponents  
133 calculated on the falling limb of the post-ISM hydrograph (see Methods) are close to 1, and suggest  
134 the contribution of a confined aquifer to discharge<sup>21</sup>. The estimated aquifer storage capacity is ~180  
135 mm per unit area, representing ~28 km<sup>3</sup> for the three main catchments of Nepal (Table 1). Modeling  
136 also indicates that the annual volume of water flowing through this groundwater system represents  
137 ~2/3 of the annual river discharge (Supplementary Table S1). The modeled storage dynamics matches  
138 the groundwater table variations observed in dug-wells, e.g. in Jhikhu Khola catchment<sup>22</sup> (Fig. 3c).

139 The ratio between calculated water storage variations (Table 1) and water table depth observed here  
140 indicates low porosity values of a few percent. We conclude from low porosity values<sup>23</sup>, confined  
141 behavior<sup>21</sup> and characteristic diffusivity values<sup>8</sup>, that the aquifer is predominantly fractured basement.  
142 Average water table variation (total annual storage capacity divided by rock porosity, considering low  
143 porosity value) is estimated to a few tens of meters in the studied catchments.

144

145 We show that the very specific climatic regime of Nepal, characterized by distinct long lasting  
146 wet and dry seasons and a major increase of precipitation during ISM (Fig. 1b and 3a), is responsible  
147 for the recharge of fractured basement aquifers. The aquifers are refilled during ISM and purged in  
148 post-ISM, leading to the annual hysteresis effect that we observed. This behavior is observed in all the  
149 studied drainage basins, independent of their size, physiographic location or main basement geology  
150 (Fig. 1, Table 1 and Supplementary Figure S6). Very little is known in Nepal about the actual aquifer,  
151 its physical properties and the relationship with tectonic structures. These appear as critical unknowns  
152 to go further into our understanding of deep groundwater influence on the Himalayan hydrological  
153 cycle, including water resources and flood hazard as well as on landslide risk due to pore-pressure  
154 saturation processes. Finally, it is noticeable that during winter (December to February) the  
155 precipitation-discharge graphs (Fig. 2b) show a systematic higher baseflow for glaciated catchments  
156 compared to unglaciated ones. Because glaciers represent an additional water storage component in  
157 some catchments, this vertical shift of the hysteresis loops of glaciated catchments reveals the  
158 contribution of glacial melt (and snow in spring) to river discharge and can be used to quantify it.  
159 From this approach (see Methods), the snow and glacier melt contribution to river discharge is  
160 estimated to be  $\sim 14 \pm 7 \text{ km}^3 \text{ yr}^{-1}$  considering the three main catchments in Nepal (Table 1), which  
161 accounts for  $\sim 10\%$  of annual river discharge. In Nepal, the volume of water flowing through fractured  
162 basement aquifer is approximately 6 times higher than the contribution of glacial and snow melt to  
163 river discharge.

164

165 **Methods**

166 **Data and data processing**

167 Precipitation is calculated using APHRODITE (Asian Precipitation Highly Resolved Observational  
168 Data Integration Towards Evaluation of Water Resources) data (<http://www.chikyu.ac.jp/precip/>).  
169 Here, we use the daily version for monsoon Asia APHRO\_MA\_V1003R1, with a spatial resolution of  
170  $0.25^\circ$ <sup>24</sup>. It is currently the best available dataset for Nepal<sup>10</sup>. We use raw river discharge data provided  
171 by the Department of Hydrology and Meteorology of Nepal DHM (see e.g. ref. 14), derived from daily  
172 stage readings and calibrated rating curves (no interpolated data are used). Potential evapotranspiration  
173 is estimated using an elevation-based model developed for Nepal<sup>17</sup>. Basin-wide snow cover is obtained  
174 from MOD10C2 version 5 (<http://nsidc.org/data/mod10c2v5.html>), with an 8-day temporal and 500m  
175 spatial resolution<sup>27</sup>. We used the monthly temperature dataset CRU TS3.0<sup>26</sup>, with  $0.5^\circ$  gridded  
176 resolution. Daily temperature is obtained from linear interpolation.

177 **Baseflow recession analysis**

178 Recession curves have been analyzed for time-series of at least 60 days, where daily rainfall is below  
179 potential evapotranspiration and cumulated rainfall < 25 mm for each recession curve. The first 15  
180 days of each recession are not considered when fitting the recession model. Both linear and non linear  
181 models are fitted to the relationship between river discharge  $Q$  and storage  $S$ :  $Q=aS^b$ . Analytically,  
182 exponent  $b$  changes from 1 when transmissivity is constant over time (most likely for confined or very  
183 deep unconfined aquifers) to 2 for unconfined flow<sup>21</sup>. Coefficient  $a$  is the inverse of the response time  
184 when  $b \sim 1$ .

185 The annual snow and glacier melt contribution is estimated from the baseflow offset between glaciated  
186 and non-glaciated basins along the discharge axis of the hysteresis plots (Fig. 2b). The scatter of  
187 baseflow within unglaciated basins ( $\sim 5$  mm/month) is considered as uncertainty. For the Mt. Everest  
188 region (here, Dudh Koshi, station 670), our estimated melt volume ( $0.6 \text{ km}^3 \text{ yr}^{-1}$ , Tab. 1) is consistent  
189 with independent glacier mass-loss estimates, measured on  $\sim 10\%$  of the glaciated area using satellite  
190 altimetry<sup>30</sup>.

191 **Hydrological modeling**



192 We consider parsimonious conceptual models at daily and monthly time scales, GR4J and GR2M  
193 (<http://www.cemagref.fr/webgr/IndexGB.htm>). The initial versions have been built up on 4 and 2  
194 parameters respectively. We added a distributed snow module based on the HBV conceptual  
195 approach<sup>20</sup>. Data scarcity and requirement of a parsimonious model structure prevented application of  
196 a more complex approach. Rainfall and temperature data are redistributed on the ETOPO2v2 (2"  
197 resolution) elevation grid. Tsep parameter separates rainfall and snowfall (Supplementary Figure S3).  
198 Fusion temperature ( $T_f$ ) is set to 0°C. Snowmelt ( $S_m$ ) is driven by a degree-day approach with a  
199 constant melting factor  $M$ ,  $S_m=M(T-T_f)$ . The snow module adds 2 parameters to the initial GR2M and  
200 GR4J models for the whole basin. Modeled snow cover fractions are validated on MODIS snow  
201 cover<sup>27</sup> extent ( $r^2=0.8$ ).

202 The modified GR2M is based on 3 storage compartments; the snow storage, soil store and routing  
203 store, interpreted as “groundwater storage” (Supplementary Figure S3). Liquid rainfall and snowmelt  
204 are partitioned into excess rainfall, actual evapotranspiration, slow percolation and water remaining in  
205 the soil store based on a single parameter. Actual ET is driven by potential ET and reservoir water  
206 availability. At monthly time scales, the routing store gathers all water and computes discharge. The  
207 model discharge calculation was modified on a physical basis to include a-priori linear behavior from  
208 recession curve analysis with variable time response  $X5$ ,  $Q=R/X5$ . GR models allow water exchanges  
209 with outside the basin (e.g. subsurface flow) computed with parameter  $X2$ . A first order estimate of  
210 groundwater flux contribution to river discharge is computed tracking water flow from the routing  
211 store of GR4J model.

212

### 213 **Modulation of hysteresis effect: Influence of precipitation undercatch, snow melt, reservoir** 214 **residence time and glacier melt on the shape of hysteresis loops**

215 The shape of the hysteresis curve is used to deduce catchment groundwater storage capacity. Forward  
216 modeling studies allow stepwise interpretation of the hysteresis shape with respect to hydrological  
217 processes or observation errors, which might have the potential to explain the hysteresis effect. The  
218 Rapti catchment (station 360 unglaciated, with no snow) is considered as a reference to test the  
219 cumulative impact of several contributions.

220 We tested:

221 1) The effect of a systematic underestimation of precipitation and snow on the shape of the hysteresis  
222 loop. Applying 30% of excess rainfall<sup>10</sup> shrinks the hysteresis along the precipitation axis (Fig. S5 a).

223 2) The impact of snow storage and delayed melting contribution to discharge, using GLDAS-NOAH  
224 model output<sup>25</sup> as a realistic a priori estimate (100 mm snow per year). Snow melt contribution drags  
225 the baseflow upward (in March, April and June) but does not change the general shape of the  
226 hysteresis loop (Fig. S5 a).

227 3) The effect of  $t_c$  on the shape of hysteresis loops. The decrease of  $t_c$  from ~45 to 10 days, and the  
228 associated decrease of the storage capacity, does not allow to reproduce the hysteresis loops observed  
229 (Fig. S5 c).

230 4) The effect of glacier melt on the shape of hysteresis loops. We considered glacier melt contribution  
231 at a constant rate and following a seasonal temperature cycle. It induces a year long vertical shift of the  
232 hysteresis curve (increased baseflow), keeping its shape intact (Fig. S5 b).

233

234

## 235 **References**

236 1. Alley, W.M., Healy, R.W., LaBaugh, J.W. & Reilly, T.E. Flow and storage in groundwater systems.  
237 *Science* **296**, 1985-1990 (2002).

238 2. Oki, T. & Kanae, S. Global hydrological cycles and world water resources. *Science* **313**, 1068-1072  
239 (2006).

240 3. Bookhagen, B. & Burbank, D.W. Toward a complete Himalayan hydrological budget:  
241 Spatiotemporal distribution of snowmelt and rainfall and their impact on river discharge. *J.*  
242 *Geophys. Res.* **115**, 1-25 (2010).

243 4. Scherler, D., Bookhagen, B. & Strecker, M.R. Spatially variable response of Himalayan glaciers to  
244 climate change affected by debris cover. *Nature Geosci.* **4**, 156-159 (2011).

- 245 5. Anderson, S.P., Dietrich, W.E. & Brimhall, G.H. Weathering profiles, mass-balance analysis, and  
246 rates of solute loss: Linkages between weathering and erosion in a small, steep catchment.  
247 *Geol. Soc. of Am. Bull.* **114**, 1143-1158 (2002).
- 248 6. Tipper, E. et al. The short term climatic sensitivity of carbonate and silicate weathering fluxes:  
249 Insight from seasonal variations in river chemistry. *Geochim. Cosmochim. Acta* **70**, 2737-2754  
250 (2006).
- 251 7. Calmels, D. et al. Contribution of deep groundwater to the weathering budget in a rapidly eroding  
252 mountain belt, Taiwan. *Earth Planet. Sci. Lett.* **303**, 48-58 (2011).
- 253 8. Montgomery, D.R. & Manga, M. Streamflow and water well responses to earthquakes. *Science* **300**,  
254 2047-2049 (2003).
- 255 9. Barros, A.P., Chiao, S., Lang, T.J., Burbank, D. & Putkonen, J. From weather to climate-Seasonal  
256 and interannual variability of storms and implications for erosion processes in the Himalaya.  
257 *Geol. Soc. Am. Spec. Pap.* **2398**, 17-38 (2006).
- 258 10. Andermann, C., Bonnet, S. & Gloaguen, R. Evaluation of precipitation data sets along the  
259 Himalayan front. *Geochem. Geophys. Geosys.* **12**, Q07023 (2011).
- 260 11. Shrestha, M.L. Interannual variation of summer monsoon rainfall over Nepal and its relation to  
261 Southern Oscillation Index. *Meteorol. Atmosph. Physics* **75**, 21-28 (2000).
- 262 12. Bookhagen, B., Thiede, R. & Strecker, M. Abnormal monsoon years and their control on erosion  
263 and sediment flux in the high, arid northwest Himalaya. *Earth Planet. Sci. Let.* **231**, 131-146  
264 (2005).
- 265 13. Immerzeel, W., Droogers, P., Dejong, S. & Bierkens, M. Large-scale monitoring of snow cover and  
266 runoff simulation in Himalayan river basins using remote sensing. *Remote Sens. Environ.* **113**,  
267 40-49 (2009).
- 268 14. Hannah, D., Kansakar, S., Gerrard, A. & Rees, G. Flow regimes of Himalayan rivers of Nepal:  
269 nature and spatial patterns. *J. Hydrol.* **308**, 18-32 (2005).

- 270 15. Bookhagen, B. & Burbank, D.W. Topography, relief, and TRMM-derived rainfall variations along  
271 the Himalaya. *Geophys. Res. Lett.* **33**, 1-5 (2006).
- 272 16. Putkonen, J.K. Continuous Snow and Rain Data at 500 to 4400 m Altitude near Annapurna, Nepal,  
273 1999–2001. *Arctic, Antarctic, and Alpine Research* **36**, 244-248 (2004).
- 274 17. Lambert, L. & Chitrakar, B. Variation of potential evapotranspiration with elevation in Nepal.  
275 *Mountain Research and Development* **9**, 145–152 (1989).
- 276 18. Mouelhi, S., Michel, C., Perrin, C. & Andreassian, V. Stepwise development of a two-parameter  
277 monthly water balance model. *J. Hydrol.* **318**, 200-214 (2006).
- 278 19. Wang, Q.J. et al. Monthly versus daily water balance models in simulating monthly runoff. *J.*  
279 *Hydrol.* **404**, 166-175 (2011).
- 280 20. Bergström, S. *The HBV Model. Computer models in watershed hydrology. V. P. Singh ed.,* 443-476  
281 (Water Resources Publications: Colorado, USA, 1995).
- 282 21. Wittenberg, H. Baseflow recession and recharge as nonlinear storage processes. *Hydrol. Processes*  
283 **13**, 715-726 (1999).
- 284 22. Dongol, B.S. et al. Shallow groundwater in a middle mountain catchment of Nepal: quantity and  
285 quality issues. *Env. Geol.* **49**, 219-229 (2005).
- 286 23. De Marsily, G. *Quantitative Hydrogeology: Groundwater Hydrology for Engineering.* (Academic  
287 Press: Orlando, 1986).
- 288 24. Yatagai, A. et al. A 44-year daily gridded precipitation dataset for Asia based on a dense network of  
289 rain gauges. *Sola* **5**, 137–140 (2009).
- 290 25. Rodell, M. et al. The Global Land Data Assimilation System. *Bulletin of the American Meteorol.*  
291 *Soc.* **85**, 381-394 (2004).
- 292 26. Mitchell, T.D. & Jones, P.D. An improved method of constructing a database of monthly climate  
293 observations and associated high-resolution grids. *Int. J. Clim.* **25**, 693-712 (2005).

- 294 27. Hall, D.K., Riggs, A.G. & Salomonson, V.V. MODIS/Terra Snow Cover 8-Day L3 Global 0.05deg  
295 CMG V005, MOD10C2. Boulder, Colorado USA: National Snow and Ice Data Center. *Digital*  
296 *media* (2006 updated daily).
- 297 28. National Snow and Ice Data Center. World glacier inventory. World Glacier Monitoring Service  
298 and National Snow and Ice Data Center/World Data Center for Glaciology, Boulder, CO.  
299 Digital media. (1999 updated 2009).
- 300 29. Department of Mines and Geology Nepal. Geological Map of Nepal. 1:1.000.000 (1994).
- 301 30. Bolch, T., Pieczonka, T. & Benn, D.I. Multi-decadal mass loss of glaciers in the Everest area  
302 (Nepal Himalaya) derived from stereo imagery. *The Cryosphere* **5**, 349-358 (2011).

303

#### 304 **Acknowledgements**

305 C.A. benefited from a 3 years PhD scholarship awarded by the German Academic Exchange Service  
306 (DAAD, D/08/42538) and from the French-German double PhD program of the French-German  
307 University Saarbrücken (DFH/UFA). The authors like to thank K. P. Sharma and his team from the  
308 Department of Hydrology and Meteorology of Nepal (DHM) for providing hydrological data and M.  
309 Dhakal from ICIMOD Nepal for sharing supplementary information on dug-well measurements.

#### 310 **Authors contributions**

311 C.A. acquired and analyzed the data. L.L. and C.A. performed the hydrological modeling. All authors  
312 discussed the results and wrote the manuscript.

#### 313 **Additional information**

314 Correspondence and requests for materials should be addressed to C.A.

315

#### 316 **Figure captions**

317 **Figure 1| Hydrological setting of the Nepal Himalayas.** a, Precipitation distribution map,  
318 hydrological discharge stations used in this study (black diamonds) and contours (red lines) of the  
319 studied drainage basins. Grey lines mark political boundaries. Mean annual precipitation rates (see

320 methods), representing 50 years of data, are draped over shaded relief. River network is displayed in  
321 blue and glaciers in white (after ref. 28). **b**, Mean basin-wide precipitation (1951-2006, in green),  
322 discharge (blue) and potential evapotranspiration (red) for the Narayani drainage basin. Bold blue line  
323 with blue shading represents the mean, maximum and minimum daily discharge over 34 years (station  
324 450). **c**, Simplified geological map of Nepal<sup>29</sup>: QS: Quaternary Sediments, SW: Siwaliks formation,  
325 LH: metasediments of the Lesser Himalayas, HCC: High Himalayan Crystalline, TSS: Tethyan  
326 Sediment Series.

327

328 **Figure 2| Precipitation-discharge (P-Q) anticlockwise hysteresis plot. a**, Bi-logarithmic P-Q plot of  
329 daily data for the Narayani basin over 34 years at station 450 (~12,300 data points). Data plotted are  
330 specific discharges (discharges normalized by drainage area) and mean basin precipitation rates. Note  
331 that discharge is not plotted when precipitation is zero. Color bar is scaled for a calendar year. White  
332 filled circles represent the mean monthly values over 34 years, the months being indicated by  
333 numbers. The error bars represent the 5% and 95% quantiles of the daily data distribution of each  
334 month. Inset shows the data filtered with a 30-day moving average. **b**, Mean annual hysteresis loops  
335 plotted from monthly mean data for all the drainage basins. Solid lines represent partially glaciated  
336 basins and dashed lines unglaciated ones (percentage of glacial coverage from ref. 28).

337

338 **Figure 3| 10-year (1997-2006) temporal variability of several hydrological compartments,**  
339 **Narayani basin. a**, Daily precipitation (green), and daily specific river discharge (blue). **b**,  
340 Temperature (orange) as a glacier melt proxy (from CRU<sup>26</sup>) and percentage of basin-wide snow cover  
341 (dark green, data from MODIS MOD10C2 v.5<sup>27</sup> with a 8-day temporal resolution). **c**, Calculated  
342 groundwater storage (red), shading illustrating model uncertainty (Supplementary Figure S2). Ground  
343 water table variation (dark blue) observed in a dug-well in Jhikhu Khola Basin<sup>22</sup> (station no. 1) from  
344 ref. 22 and unpublished data provided by these authors. The abnormal low water table in 2004 likely  
345 results from exhaustive exploitation.

346

347

348 **Table 1| Properties of the studied drainage basins and summary of results (monthly modeling).**

349 Maximum elevation is used as a proxy for snow occurrence during winter (considering winter  
350 snowline at ~3000 m asl.<sup>16</sup>). Precipitation rate is computed as a mean basin value. Specific discharge is  
351 computed from daily river gauge data. Real-evapotranspiration ETR is computed from our modeling  
352 (see Methods). Storage represents the mean annual amplitude of storage variation and its respective  
353 uncertainty in km<sup>3</sup> and mm respectively (Supplementary Figure S2).  $t_c$  is the characteristic basin  
354 response time, derived from hydrological modeling or from the recession curve of hydrographs (see  
355 Methods). The % glaciated values are calculated using data from ref. 28. Ice melt is the annual  
356 volumetric glacier ice melt contribution to the rivers, estimated from the relative baseflow shift in the  
357 precipitation-discharge plot (Fig. 2b). % snow-melt is the contribution of snow to discharge (both  
358 directly and via the aquifer).

359

#### 360 **Supplementary Figure**

361 **S1| Difference between strong and weak monsoon hysteresis loops.** Precipitation-discharge  
362 hysteresis loop for the strong monsoon year 1999 and the weak monsoon year 1997<sup>11</sup> for the Narayani  
363 Basin. Data has been filtered with a 5-day moving average to avoid small-scale noise. The amplitude  
364 of the hysteresis loop is larger during strong monsoon years compared to weak ones. Q/A is the  
365 specific discharge, P is the mean basin precipitation.

366

367 **S2| 10-year (1997-2006) temporal variability of several hydrological discharge cycle**  
368 **compartments, Koshi Basin (I) and Karnali Basin (II), central Nepal.** **a**, Daily precipitation  
369 (green), and daily specific river discharge (blue). **b**, Temperature (orange) as a glacier melt proxy  
370 (from CRU<sup>26</sup>) and percentage of basin-wide snow cover (dark green, data from MOD10C2 v.5<sup>27</sup> with  
371 an 8-day temporal resolution). **c**, Calculated groundwater storage evolution (red) derived from a  
372 modified version of the conceptual hydrological model GR2M<sup>18</sup> (see methods), shading illustrating  
373 model uncertainty, and ground water table variation (dark blue) observed in dug-wells in the Jhikhu  
374 Khola Basin<sup>22</sup> (station no. 1).

375 **Uncertainty estimation:**

376 A Monte-Carlo approach is carried out to quantify the impact of observation data uncertainties on  
377 modeled groundwater properties (storage capacity, response time, see Table 1). Multiplicative errors  
378 have been considered for rainfall and discharge. Rainfall might be systematically underestimated by  
379 30%±10, and discharge biased by ±5%. Conversely, ET and temperature errors are taken as additive,  
380 based on differences between independent datasets. Model is then recalibrated, model structure error is  
381 therefore not considered in this uncertainty analysis. While groundwater storage capacity is highly  
382 sensitive to systematic bias in precipitation data, recession curves, and therefore time response, are  
383 rather well constrained (Table 1).

384

### 385 **S3| Flowchart of the modified version of the conceptual hydrological model used in this study.**

386 Simplified schema of the conceptual models GR2M and GR4J<sup>18</sup>, and the added snow module. Black  
387 lines applied for both models GR2M and GR4J whereas gray dotted lines applied only for model  
388 GR4J. Please refer to Mouelhi et al. 2006 (ref. 18), the method section and the following web  
389 resource <http://www.cemagref.fr/webgr/Modelesgb/descriptionsgb.htm> for more detailed information.

390

391 **S4| Modeled vs. observed hysteresis loop for Narayani catchment (450).** Data are plotted on a  
392 monthly scale. The inset shows the linear correlation between the observed and modeled discharge.  
393 Q/A is the specific discharge. P is the monthly basin-wide precipitation rate.

394

### 395 **S 5| Influence of precipitation undercatch, snow melt, reservoir residence time and glacier melt**

396 **on the shape of hysteresis loops.** The months are indicated by numbers. In all the examples, the mean  
397 monthly precipitation-discharge values for Rapti River at station 360 are used as a reference (blue). **a,**  
398 Effect of a constant 30% undercatch of precipitation and impact of snowmelt contribution, considering  
399 an annual water equivalent of the snowmelt contribution after the GLDAS-NOAH model<sup>25</sup> (inset). **b,**  
400 Impact of the basin-wide storage capacity on the hysteresis shape of the Rapti catchment, considering  
401 characteristic basin response times of 35 days and of only 10 days, corresponding to a 20-fold  
402 downsizing of the storage capacity (see Methods). **c,** Influence of a 100 mm yr<sup>-1</sup> glacier melt



403 contribution (or storage), considering a constant melt rate, equally distributed over the whole year or  
404 assuming a cyclic, temperature-driven ice melt contribution (both illustrated in the inset).

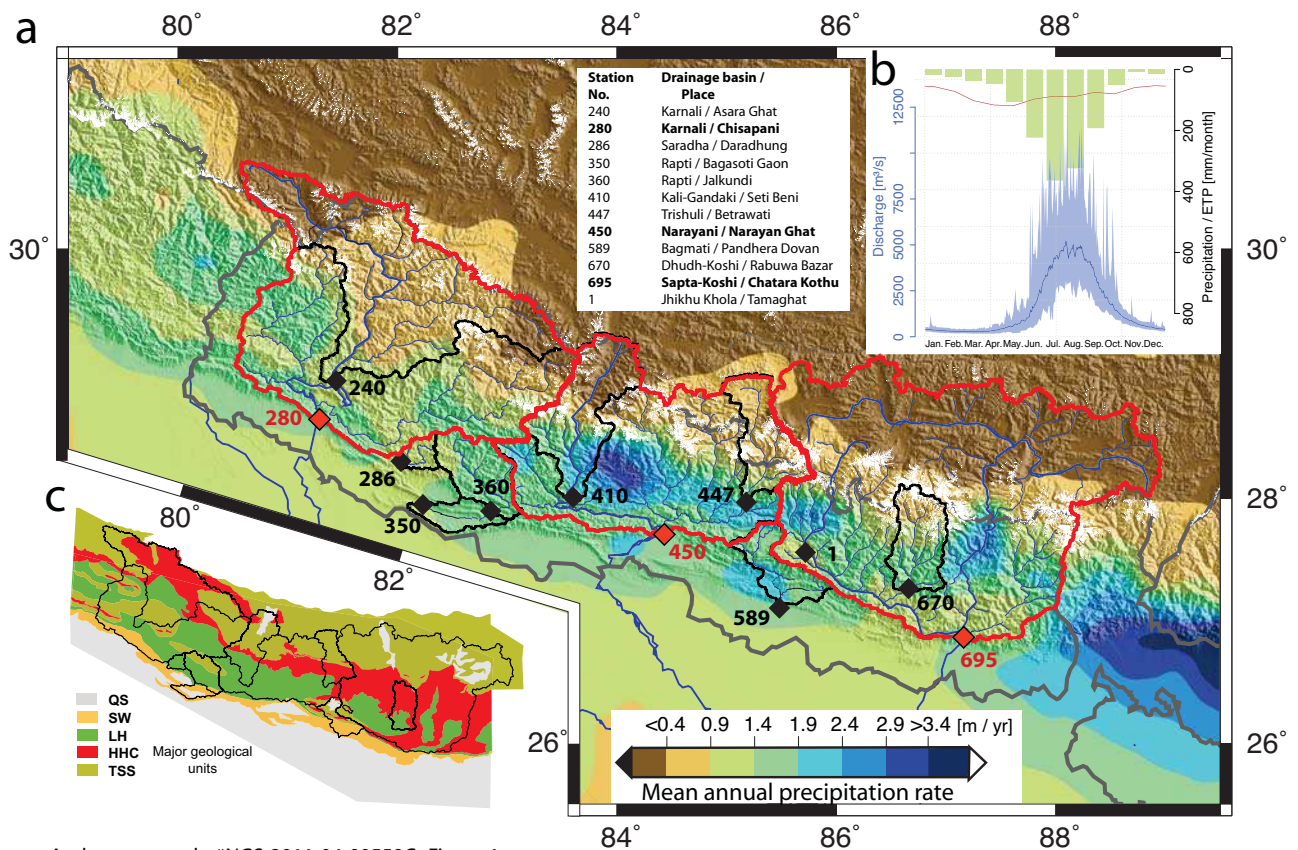
405

406 **S6 | Comparison between groundwater storage properties and geological units within the studied**  
407 **drainage basins.** Graphs illustrate storage properties (response time and storage capacity), plotted  
408 against geological unites.

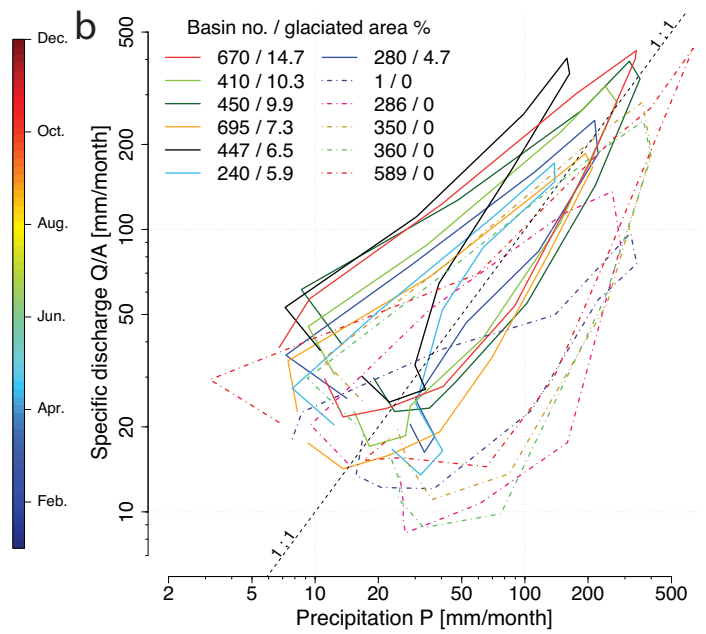
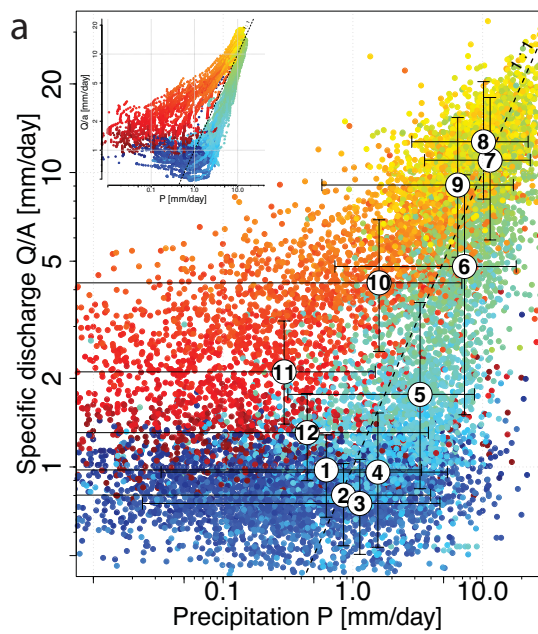
409

410 **Table S1| Properties of the studied drainage basins and summary of results (daily modeling).**

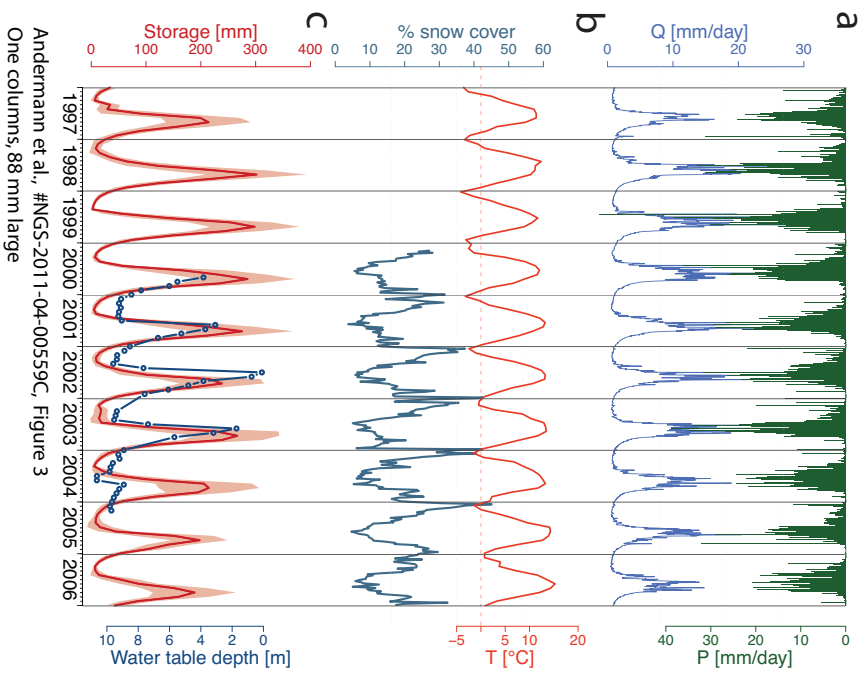
411 Real-evapotranspiration ETR, is computed from the conceptual model GR4J<sup>18</sup> on the basis of potential  
412 evapotranspiration<sup>17</sup>. The storage represents the mean annual amplitude of storage variation and its  
413 respective uncertainty (Supplementary Figure S2), in km<sup>3</sup> and mm respectively.  $t_c$  is the characteristic  
414 basin response time derived from the model GR4J and the recession curve of the falling limb of the  
415 hydrographs. % snow-melt is the contribution of snow to discharge (both directly and via the aquifer).  
416 The retarded discharge represents groundwater contribution to the river discharge and is expressed as  
417 percent of the annual river discharge.



Andermann et al., #NGS-2011-04-00559C, Figure 1  
Two columns, 170 mm large



Andermann et al., #NGS-2011-04-00559C, Figure 2  
Two columns, 170 mm large



Andermann et al., #NGS-2011-04-00559C, Figure 3  
 One column, 88 mm large

Station No.	240	<b>280</b>	286	350	360	410	447	<b>450</b>	670	<b>695</b>	589	1
Basin	Karnali	<b>Karnali</b>	Saradha	Rapti	Rapti	Kali Gandaki	Trishuli	<b>Narayani</b>	Dudh Koshi	<b>Sapta Koshi</b>	Bagmati	Jhikhu Khola
Lat [°]	28.95	<b>28.64</b>	28.64	27.90	27.95	28.01	27.97	<b>27.71</b>	27.27	<b>26.87</b>	27.11	27.59
Long [°]	81.44	<b>81.29</b>	82.03	82.85	82.23	83.60	85.18	<b>84.43</b>	86.66	<b>87.16</b>	85.48	85.67
Size [km <sup>2</sup> ]	21121	<b>45967</b>	808	3648	5198	7169	4428	<b>32002</b>	3880	<b>57719</b>	2849	111
Precipitation [mm yr <sup>-1</sup> ]	558	<b>920</b>	1107	1522	1470	1030	692	<b>1396</b>	1295	<b>920</b>	1932	1285
Discharge [mm yr <sup>-1</sup> ]	650	<b>789</b>	460	903	787	1145	1513	<b>1145</b>	1598	<b>1039</b>	1205	374
ETR [mm yr <sup>-1</sup> ]	176	<b>234</b>	656	720	654	178	121	<b>367</b>	178	<b>179</b>	839	171
Availability of discharge	1975-2006	<b>1973-2006</b>	1976-2006	1978-2006	1985-2006	1979-1995	1977-2006	<b>1973-2006</b>	1987-2006	<b>1977-2006</b>	2001-2006	1998-2006
%Area glaciated	5.9	<b>4.7</b>	0.0	0.0	0.0	10.3	6.5	<b>9.9</b>	14.7	<b>7.3</b>	0.0	0.0
Max Elevation [m asl.]	7549	<b>7697</b>	2800	3623	3623	8147	7352	<b>8147</b>	8848	<b>8848</b>	2795	2200
Nash-Sutcliffe coef.	0.93	<b>0.92</b>	0.79	0.88	0.95	0.91	0.79	<b>0.91</b>	0.94	<b>0.89</b>	0.88	0.29
Recession exp. $b$ ( $Q=aS^b$ )*	1.01	<b>1.11</b>	1.16	1.01	1.18	1.01	1.02	<b>1.16</b>	1.17	<b>1.01</b>	1.12	1.18
Storage capacity [km <sup>3</sup> ]	3.1 ±1.2	<b>8.1 ±3.3</b>	0.21 ±0.08	1.6 ±0.7	1.8 ±0.8	1.3 ±0.6	0.9 ±0.4	<b>9.9 ±3</b>	1.2 ±0.4	<b>10.3 ±6</b>	1.2 ±0.5	0.03 ±0.01
Storage capacity [mm]	150±60	<b>175±70</b>	260±90	430±180	350±150	180±80	200±80	<b>310±125</b>	300±105	<b>180±100</b>	440±180	300±120
$t_c$ GR2M [days]*	46 ±5	<b>50 ±5</b>	37 ±3	36 ±8	41 ±8	45 ±4	38 ±4	<b>50 ±5</b>	53 ±11	<b>47 ±4</b>	30 ±5	120 ±35
$t_c$ recession curve [days]*	40 ±10	<b>46 ±15</b>	37 ±13	44 ±17	42 ±15	41 ±15	44 ±11	<b>40 ±13</b>	45 ±9	<b>41 ±11</b>	41 ±19	77 ±24
Ice+snow melt [km <sup>3</sup> yr <sup>-1</sup> ]	1.2	<b>4.1</b>	n.a.	n.a.	n.a.	0.7	0.8	<b>5.3</b>	0.6	<b>4.1</b>	n.a.	n.a.
% snow-melt	12	<b>7</b>	n.a.	n.a.	n.a.	3	13	<b>2</b>	6	<b>5</b>	n.a.	n.a.
Geology units % coverage QS/SW/LH/HHC/TSS	0/0/17/44/39	<b>0/5/33/25/37</b>	0/3/96/0/1	0/5/62/0/33	8/24/45/0/23	10/0/32/15/4 3	0/0/8/37/55	<b>2/0/42/23/33</b>	0/0/26/73/1	<b>6/0/16/40/38</b>	13/42/2/11/3 2	0/0/11/17/72

\* see Methods